Bright Cathodoluminescent Thin Films for Scanning Nano-Optical Excitation and Imaging

David M. Kaz,[†,⊥] Connor G. Bischak,[†] Craig L. Hetherington,[†] Hannah H. Howard,[†] Xavier Marti,[§] James D. Clarkson,[§] Carolina Adamo,[▽,¶] Darrell G. Schlom,[▽,⊗] Ramamoorthy Ramesh,[‡,§,∥] Shaul Aloni,[∥,#] D. Frank Ogletree,[∥,#] and Naomi S. Ginsberg[†,‡,⊥,∥,○,*]

[†]Department of Chemistry, [‡]Department of Physics, and [§]Department of Materials Science and Engineering, University of California, Berkeley, California 94720, United States, [⊥]Physical Biosciences Division, [∥]Materials Science Division, and [#]Molecular Foundry, Lawrence Berkeley National Laboratory, Berkeley, California 94720, United States, [▽]Department of Materials Science and Engineering, Cornell University, Ithaca, New York 14853, United States, [⊗]Kavli Institute at Cornell for Nanoscale Science, Ithaca, New York, 14853, United States, and [○]Kavli Energy NanoSciences Institute, Berkeley, California 94720, United States. [¶]Present address: Geballe Laboratory for Advanced Materials, Stanford University, Stanford, CA 94305, United States.

ABSTRACT Demand for visualizing nanoscale dynamics in biological and advanced materials continues to drive the development of subdiffraction optical probes. While many strategies employ scanning tips for this purpose, we instead exploit a focused electron beam to create scannable nanoscale optical excitations in an epitaxially grown thin-film of cerium-doped yttrium aluminum perovskite, whose cathodoluminescence response is bright, robust, and spatially resolved to 18 nm. We also demonstrate lithographic patterning of the film's luminescence at the nanoscale. We anticipate that converting these films into free-standing membranes will yield a powerful near-field optical microscopy without the complication of mechanical scanning.

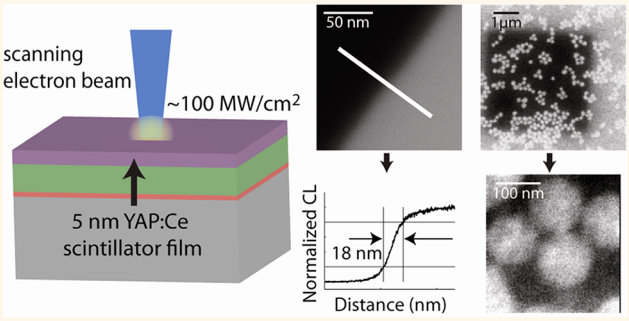

KEYWORDS: cathodoluminescence · thin-films · nano-optical · near-field · imaging · nanopatterning

Because the structure and dynamics of complex systems are often characterized by length scales below the wavelength of visible light, subdiffraction optical probes have been highly sought after for applications in high-resolution imaging of solid state materials, soft matter and biological samples. Far-field approaches such as stimulated emission depletion (STED) microscopy,[1] structured illumination microscopy,[2] and stochastic localization techniques[3−5] have flourished in recent years. A variety of optical near-field approaches[6−9] also exist, including static structures such as solid immersion lenses,[10] zero-mode waveguides,[11,12] and plasmonic nanostructures.[13−16] Several of these innovations have been integrated with physical tips that can be rastered over a sample to form an image.[17−22] Yet, to capture high-fidelity spatial information without tip perturbations or contact-based sample damage requires moving beyond traditional mechanical scanning.

Electron beams are routinely focused to the nanometer scale and scanned electronically to obtain nanoscale images of robust samples, albeit without spectral selectivity. To leverage the tight focus of an electron beam for noninvasive optical excitation, we have developed an ultrathin scintillating film of cerium-doped yttrium aluminum perovskite ($YAlO_3$:Ce, or YAP:Ce) that acts as a bright, nanoscale optical source when excited by a tightly focused electron beam. By rastering over the film in a scanning electron microscope (SEM) (Figure 1), the optical spot generated in the thin film could be used to rapidly acquire high-resolution images without any mechanical moving parts or tip−surface interactions. We anticipate performing spectrally selective optical excitation and imaging of thin biological, fluid or solid-state samples in proximity to the scintillating film. Ultimately, to realize the geometry necessary for imaging, both sides of the film must be exposed.

* Address correspondence to nsginsberg@berkeley.edu.

Received for review September 19, 2013 and accepted October 22, 2013.

Published online October 25, 2013
10.1021/nn404911a

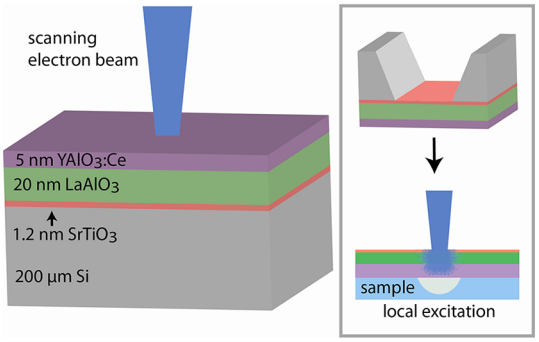

Figure 1. Schematic of YAP:Ce scintillating film on the Si/STO/LAO substrate. In all measurements, the electron beam impinges directly on the YAP:Ce (also known as $YAlO_3$:Ce) film. (Inset) For imaging applications, both sides of the YAP:Ce film must be exposed by removing the Si layer (top) so that the electron beam can access the STO side of the film and so that a sample can be placed on the opposite side adjacent to the YAP:Ce film (bottom).

As illustrated in the inset of Figure 1, one side abuts the sample while the electron beam impinges on the other side. Here, we describe our first significant advance toward this imaging platform: fabricating a scintillating thin film, characterizing its luminescent response, and establishing its suitability as a nanoscale optical source.

YAP:Ce is a robust, highly efficient inorganic scintillator used in a range of detection applications including scanning electron microscopy.[23] When they are excited by an electron beam, scintillating materials cathodoluminesce. That is, they emit light due to energy deposition from inelastic electron scattering within the material.[24] The shape and extent of the optically active volume depends on the accelerating voltage and diameter of the electron beam, as well as on the material properties. Cathodoluminescence (CL) has been used to study the physical properties of nanoparticles,[25−27] nanoantennae,[28,29] and nanowires.[30,31] There are, however, only a handful of very recent studies in which CL has been utilized for illumination.[32−34]

In YAP:Ce, Ce^{3+} dopants substitute for a small fraction of yttrium ions in the orthorhombic perovskite lattice and are responsible for the scintillator's luminescence. When electrons impinge on a YAP:Ce lattice, excitons generated in the lattice are trapped at the Ce^{3+} dopants.[35] Recombination occurs on the Ce^{3+} 5d to 4f transition, which is dipole-allowed and has a 25 ns emission decay lifetime in bulk,[36] orders of magnitude shorter than most inorganic scintillators, which could enable the extremely rapid response needed for high frame-rate, or time-resolved, imaging. In contrast to many other cathodoluminescent materials that have multiple emission lines throughout the visible spectrum, YAP:Ce has a single CL peak centered at 370 nm,[37] making it ideal as a spectrally selective illumination source for photoexcitation.

Nanoscale films of notable scintillators, including Er- and Nd-doped YAP, have been fabricated using a variety of deposition techniques.[38−46] Yet, many of these scintillating films possess characteristics unsuitable for use as a scanning nanoscale optical source, such as a long excited state lifetime, a polychromatic CL spectrum, decomposition under electron beam bombardment, or poor crystallinity. In contrast, YAP:Ce has a short lifetime, cathodoluminesces in a single band, and is robust to electron beam bombardment. Until now, however, YAP:Ce had not been grown as a nanoscale epitaxial thin film.

Here, we present the fabrication and characterization of an extremely bright cathodoluminescent nanoscale optical source composed of an ultrathin, epitaxial, film of YAP:Ce. By exciting the film with a focused electron beam, in the configuration shown in Figure 1, we have demonstrated a CL spatial resolution at least as good as 18 nm, luminescence that produces near-field optical intensities as high as 100 MW/cm^2, the ability to control the emission spectrum *via* film thickness, and the capability to pattern the luminescence on the nanoscale. The film constitutes a bright, robust, rapidly scannable, spectrally selective, nanoscale optical source when stimulated with a low-energy electron beam, and shows strong potential for nanoscale excitation and imaging.

RESULTS AND DISCUSSION

YAP:Ce Film Quality. High-quality films of YAP:Ce ranging in thickness from 4 to 63 nm were grown *via* pulsed laser deposition (PLD) onto silicon substrates with buffer layers of strontium titanate ($SrTiO_3$, or STO) and lanthanum aluminate ($LaAlO_3$, or LAO) (Figure 1) and, as a control, on bulk crystalline LAO substrates. The buffer layers, deposited by molecular-beam epitaxy (MBE),[47,48] facilitate the growth of crystalline YAP:Ce, preserving the bulk crystalline YAP:Ce brightness and emission spectrum. All films were confirmed to be highly epitaxial by identifying strong peaks in X-ray diffraction (XRD) $\theta - 2\theta$ scans corresponding to diffraction from the (001) lattice planes in YAP:Ce (Supporting Information Figures S1 and S2). X-ray diffraction revealed no traces of spurious phases or additional crystal orientations. Rocking curves show that the YAP:Ce films are at least as crystalline as the buffer layers (Supporting Information Figure S3). The cerium dopant concentration in the films was measured with Rutherford backscattering (RBS) to be 0.55 wt %, identical to that of the source material (Supporting Information Figure S4). Surface roughness, as measured by atomic force microscopy (AFM), was on the order of 0.2−0.5 nm rms over 25 μm^2 (Supporting Information Figure S5). Additionally, the spectra and lifetimes of photoluminescence from films were measured and closely resemble those of bulk YAP:Ce (Supporting Information Figures S6 and S7).[49] Thus, the YAP:Ce films possess the requisite crystal structure, composition, and quality that are critical to obtaining

bright cathodoluminescence with the desired spectral character.

CL Brightness and Stability. Nanoscale optical spots were generated in a 5-nm-thick YAP:Ce film under excitation from a 20-keV electron beam in order to characterize the brightness and robustness of the film's CL. A moderate beam current of 0.27 nA generated a total emitted power in 4π sr of 22 pW, and the emitted power generally increased with current. We separately confirmed that the bare Si/STO/LAO substrates do not cathodoluminesce.

To assess the brightness of an optical spot when acting as a near-field illumination source for a sample near the film surface, we calculated the intensity of local fields based on the measured far-field emission power. The full calculation is contained in the Supporting Information. Briefly, according to Monte Carlo simulations of 20-keV electrons scattering in the 5-nm thick films, performed using the CASINO software package[50] (Supporting Information Figures S8 and S9), 86% of the electron beam energy deposited in the film is deposited in a roughly cylindrical volume within a radius equal to the $1/e^2$ radius of the beam. We assume that this cylinder also represents the optically active volume. Thus, for the 0.27 nA beam, this active volume was 6.4 nm in radius and contained on average 85 luminescent Ce ions. For these parameters, we derive a total photon emission rate of 38.5 MHz from the measured emitted power, adjusted for collection efficiency, and hence a mean emission rate per Ce ion of about 400 kHz. The near-field intensity at the film surface is calculated, based on the form of nonradiative fields around an oscillating dipole, from this measurement of the radiated energy (Supporting Information Figure S10). We obtain a value of about 24 MW/cm^2, similar to intensities in plasmonically enhanced near-field microscopy[13] and about 1000 times the dye-saturating intensity used in confocal microscopy. The optical intensity is also similar to that on the surface of a 6-nm CdSe/ZnS quantum dot driven to saturation. Unlike point optical sources, however, YAP:Ce notably does not dim over many minutes of excitation (see Supporting Information for details).

To determine the maximum brightness of the YAP:Ce film, the beam current was increased in two steps. At a 2.9 nA current (with an associated 2.7-nm beam diameter), the total power output was 160 pW, yielding an average emission rate per Ce of 14 MHz. At 11.3 nA (4.4-nm beam diameter), the emission was 340 pW total, for a rate per Ce of 12 MHz. Furthermore, since the electron flux at the center of each beam was higher than at the edges, the emission rates at the active volume centers must be even higher than the average emission rates determined above. Given that these rates are within error of each other despite a 50% difference in the respective currents applied per unit area, it is likely that YAP:Ce CL is saturated at such levels. As further corroboration, these rates approach the inverse of the ~25 ns CL lifetime previously reported.[36] Nevertheless, as the emission rate can still be tuned from kilohertz all the way up to megahertz by varying the current, we expect that the excitation rate for fluorophores at or near the film surface can be adjusted with high dynamic range to easily suit typical experimental requirements.

While 20-keV electrons can fully penetrate and pass through the film, lower-energy electrons may be more useful for imaging applications because they penetrate less deeply (Supporting Information Figure S9). Therefore, we measured the CL power under 10-keV and 2-keV beams to confirm the high brightness of YAP:Ce films at lower voltages. At 10 kV, a moderate current of 0.18 nA yielded an emission rate per Ce of 570 kHz, and at 2 kV and 2.83 nA, a rate per Ce of 1 MHz was measured. These figures are similar to the 400 kHz−14 MHz emission rates reported above for the 20-keV beams. Thus, the beam accelerating voltage can also be tailored to suit a particular application without any additional limitations on the optical intensity.

The above measurements and estimates demonstrate how the robustness and CL intensity of the YAP:Ce film make it attractive as an easily scannable near-field source for local excitation and imaging at the nanoscale. Since the near-field excitation probability falls off as the inverse of distance to the sixth power, the near-field excitation region has a nanoscale axial extent and has lateral dimensions dictated by the size of the active volume in the film. Perhaps most importantly for imaging, the extraordinary brightness of the optical spot will allow the use of short pixel residence times, which will in turn permit image acquisition at extremely high rates limited only by the illuminated sample's photophysics.

CL Spatial Resolution. To use a YAP:Ce film as a nanoscale optical source for imaging, the extent of the optical field in the film generated by an electron beam must be confined to a spot size not much larger than the electron beam itself. As a verification, the lateral resolution of CL in the YAP:Ce films was determined by measuring the brightness profile of CL across a physically sharp edge cleaved in a 5-nm-thick film, as illustrated in Figure 2. Representative images recorded with CL and secondary electrons (SE) are shown in Figure 2, panels a and b, respectively. The corresponding line cuts of the CL and SE intensity are plotted in Figure 2c,d.

The 80/20 width of the film's step edge (the distance between points in the trace corresponding to 20% and 80% of the step height) measured by SE detection with a 20-keV beam is 10 nm. The width of the same edge as obtained by analyzing the CL image is 18 nm. The SE profile in Figure 2d includes a slight overshoot of the maximum signal level as the electron beam crosses the boundary. This feature is a

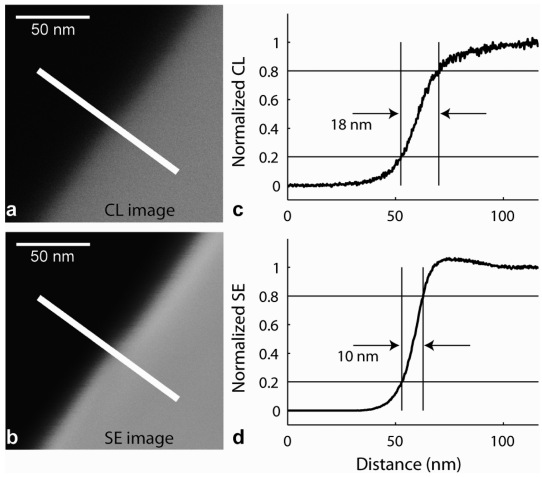

Figure 2. Comparison of CL resolution with secondary electron (SE) resolution. A 20-keV, 4.4-nm-diameter electron beam was rastered over the cleaved edge of a 5-nm-thick YAP:Ce film. Simultaneous images were acquired using (a) CL detection and (b) SE detection. (c and d) Line profiles across the edge in each image indicate the resolution of the two detection methods is comparable. The slight overshoot in the SE intensity profile is an artifact due to increased secondary electron yield area along the cleaved face and results in an underestimate of the SE width.

well-known artifact associated with electron imaging near steep edges, where additional secondary electrons escape the material through its side face,[51] creating the illusion of higher resolution. In light of this overshoot effect, the resolution of the step measured by CL appears very close to that measured by SE. In both cases, since the measured signal width is a convolution of the electron beam profile with the physical profile of the cleaved film edge, any physical imperfections in the edge can limit the measurement of the spot size. Thus, we conclude that the CL resolution at 20 kV is at least as good as 18 nm. For optical imaging applications, this resolution within YAP:Ce corresponds to the lateral extent of the region that could transfer energy to nearby chromophores in a sample. Therefore, we expect the imaging resolution achievable with this light source to also be on the order of 18 nm, opening up the possibility to obtain extremely high-resolution optical images with the rapid scan rates of an electron beam.

CL Spectral Properties. We have further observed a controllable shift in the cathodoluminescence spectrum for the films of YAP:Ce grown on the Si/STO/LAO substrates. This shift is directly correlated to the film thickness and to the electron accelerating voltage used to generate the CL. This effect is most pronounced at low accelerating voltages for which penetration into the film is minimal—around 10 nm at 1 kV according to Monte Carlo simulations (Supporting Information Figure S9).

Emission spectra resulting from 1-keV excitation of three films of different thicknesses are plotted in Figure 3a. The 4.3-, 18-, and 46-nm films peak at wavelengths of 367, 375, and 384 nm, respectively.

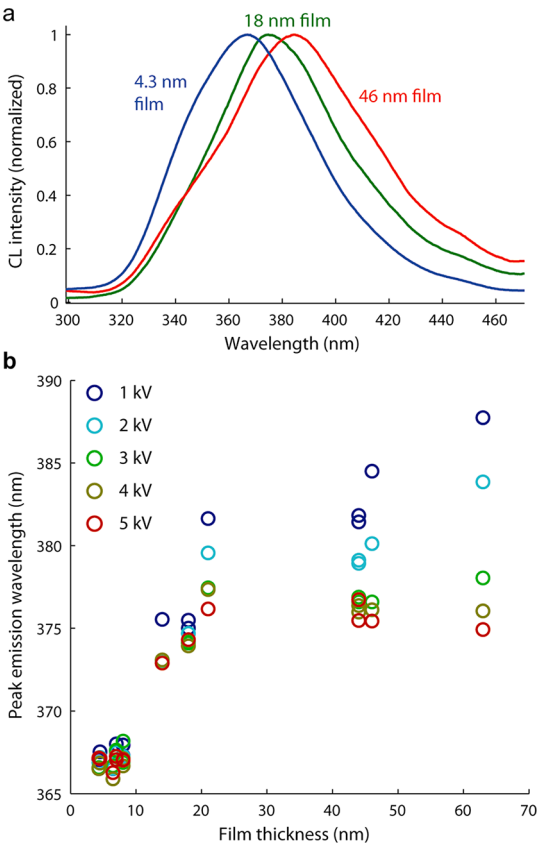

Figure 3. Variation in CL spectra as a function of film thickness and accelerating voltage. (a) CL spectra acquired with a 1-keV electron beam for a few representative films. Thicker films yield redder spectra. (b) Peak wavelength *versus* film thickness as a function of beam voltage. Higher beam voltages correspond to greater excitation depth.

A comparison of these spectra reveals that the surfaces of thicker films have progressively more red-shifted emission. To incrementally probe deeper into the films, we swept the accelerating voltage up to 5 kV, at which point emission occurs throughout the entire thickness of each YAP:Ce film. As shown in Figure 3b, while the thinnest films have a peak emission wavelength of 366 nm at 1−5 kV, the thickest ones have peak emission wavelengths ranging from 375 nm for a 5-keV electron beam to 388 nm for a 1-keV electron beam. This trend indicates that the local spectral properties within a film are a function of an emitter's position with respect to the LAO interface as opposed to its position with respect to the outer YAP:Ce surface.

We ruled out the possibility that the 3% lattice mismatch between LAO and YAP:Ce lattices could cause a spectral shift *via* strain gradients, as YAP:Ce films of different thicknesses on bulk crystalline LAO exhibit no spectral variation (Supporting Information Figure S11). The main difference between bulk-LAO-templated and Si/STO/LAO-templated films is revealed in substantial broadening in the rocking curves of films grown on the latter epitaxial template (Supporting Information Figure S3). This difference can be ascribed

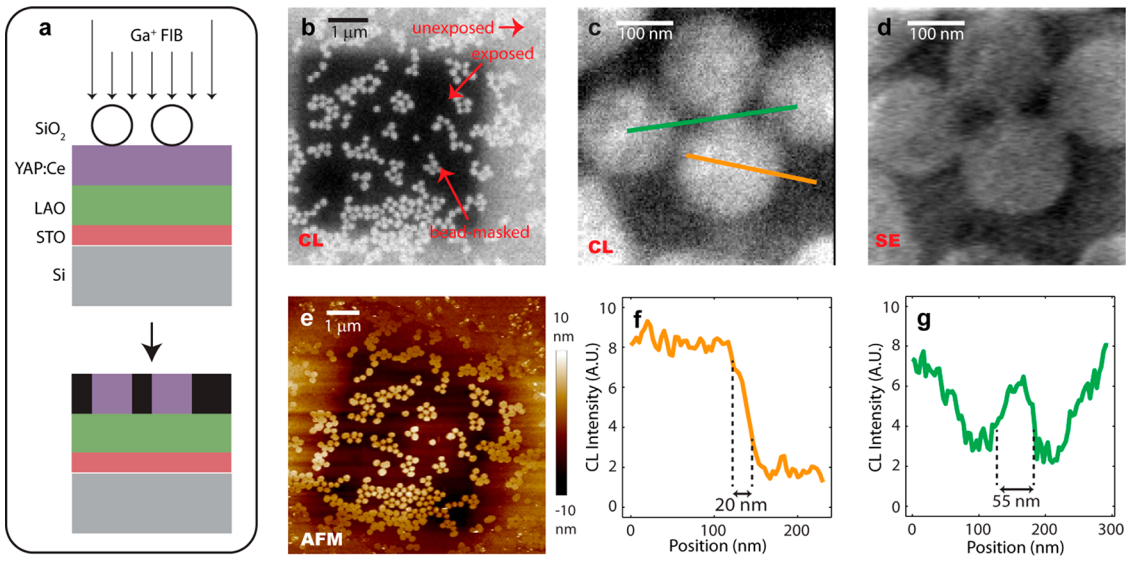

Figure 4. Nanopatterning of CL: (a) Raster-scanned focused gallium ion beam used to extinguish luminescence of a YAP:Ce film masked with 200-nm silica beads, yielding small regions of luminescent YAP:Ce; (b) CL image of a representative region after FIB and bead removal revealing clearly defined spots; (c) CL image at high resolution; (d) in-lens scattered electron image collected simultaneously with panel c; (e) AFM of the same region as in panel b; (f) profile over an edge of a milled region (orange line in panel c) indicating an apparent edge width ~20 nm in CL; (g) two dark regions, separated by ~55 nm, easily distinguished using CL (green line in panel c). In both (f) and (g), background CL intensity measured at a nearby dark area has been subtracted.

to a higher concentration of structural defects such as a high dislocation density in the LAO layer and YAP:Ce film. Because of the charged nature of dislocations in ionic materials, dislocations are associated with higher local populations of cationic or anionic vacancies.[52,53] Cationic vacancies in YAP:Ce are known to form stable pairs with nonluminescent Ce^{4+} ions,[55] and Ce^{4+} ions have been shown to quench the blue edge of the luminescence of Ce^{3+} ions in aqueous solution.[54] This quenching causes an apparent red shift in the Ce^{3+} emission spectrum.

Therefore, the red shift that we observe in the films' CL spectra could be due to an increase in the concentration of Ce^{4+} as a function of distance from the LAO interface. This hypothesis is further supported by fluorescence lifetime measurements on films of varying thickness (Supporting Information Figure S7) in which thicker films exhibit progressively shorter lifetimes, indicating increased quenching. Irrespective of the mechanism, our understanding of the YAP:Ce film emission properties enables us to control the spectral variation by careful manipulation of film thickness.

Nanopatterning of CL. For certain applications such as nanolithography, a spatially fixed nanoscale excitation volume, rather than a scannable spot, may be preferred. This scheme could be simplified if the scintillating film's optical properties could be selectively patterned such that it is optically active only at certain locations; in such a case, only predetermined nanoscale spots would luminesce even if a much wider area were excited with a defocused electron beam. To realize this objective, we developed a method for patterning the luminescence of a film at the nanoscale with a gallium focused-ion beam (FIB).

Exposure of a 20-nm-thick film to a low-energy (8 keV) FIB (Figure 4a) extinguished the film's luminescence. At high doses, the YAP:Ce film is ablated to a depth linearly dependent on dose (Supporting Information Figure S12). Yet, even at low doses, insufficient to cleanly ablate more than a few nanometers of YAP:Ce, the luminescence of the film is greatly diminished (Figure 4b,c). This extremely effective "nanoburning" of the film is likely due to local disordering of the perovskite crystal or to deep implantation of gallium ions (Supporting Information Figure S12).

We demonstrated the precision of this burning technique by first exposing the 20-nm film to the gallium beam through a mask comprising dispersed 200-nm silica beads, and by then removing the beads and capturing images with CL (Figure 4b,c), SE (Figure 4d) and AFM (Figure 4e). Analysis of these images reveals an 80/20 edge-width as narrow as 20 nm (Figure 4f), on par with the 18-nm resolution of the CL imaging. The bead mask allowed the formation of dark features spaced ~50 nm apart, and these can be clearly distinguished in CL (Figure 4g). On the basis of the sharpness of the features in Figure 4c, we estimate that dark patches could be distinguished at distances as small as 20 nm, and by using even smaller particles as masks, luminescent features of that size could be patterned into the film.

These observations show that light can be produced at controllable, local spots far smaller than a wavelength even if electron bombardment takes place

across a wider area. Thus, a combination of nanoburned films with wide-field electron excitation could transform the usual procedure of rastering a single active volume across a sample in series into the process of addressing multiple nanoscale spots in parallel. Moreover, because CL is correlated with photoluminescence (Supporting Information Figure S6), these spots could alternatively be excited through far-field optical illumination to convert far-field light into spectrally distinct, highly local near-fields. Thus, our YAP:Ce films could be used for nanoscale optical generation in two complementary modes: focused scanning cathodoluminescence mode, or a wide-field mode, driven by either electron excitation or optical illumination.

CONCLUSIONS

In summary, we have demonstrated a rapidly and easily scanned, bright, spectrally selective nanoscale optical source for optical excitation and imaging. To do so, we developed an ultrathin, epitaxial film of a YAP:Ce scintillator, whose maximum brightness when excited with a low energy electron beam is competitive with the brightest subdiffraction optical sources in use today. The CL spectral properties and the 18-nm spatial resolution achievable in these films will allow for studies of nanoscale heterogeneity of complex materials deposited on or near the YAP:Ce film. We also demonstrated that film luminescence can be patterned in order to structure sample illumination at the nanoscale.

These functionalities point to exciting opportunities in both materials and biological research. For example, with a free-standing membrane geometry (Figure 1 inset), one could deposit thin film samples onto the YAP:Ce surface using standard techniques for deposition on oxide surfaces and address the samples with CL excitation generated by an electron beam striking the opposite face. In this way, one could optically excite the samples to characterize their functional properties at length scales commensurate with their heterogeneity and on time scales that enable resolution of their dynamics. In biological applications, fluorescently labeled biomolecules in an aqueous environment encapsulated near the YAP:Ce surface could be resolved at the nanoscale in real time to reveal diffusive behavior, conformational changes or mechanical function. More generally, our approach could provide a way to address many unanswered questions about the arrangements and dynamics of liquid-phase molecules on the nanometer scale in outstanding surface chemistry problems including the electrochemical double layer, catalysis and dynamic wetting. In materials applications, one could even imagine uncovering the relationship between film morphology and device efficiency by locally triggering an optical response in photovoltaic energy transduction.

METHODS

Pulsed-laser deposition (PLD) was used to grow epitaxial films of YAP:Ce (001) on previously prepared substrates, each consisting of a 100 or 200 μm-thick silicon wafer (100) with a 4 unit-cell thick layer of strontium titanate (001) (STO) and a 20-nm thick layer of lanthanum aluminate (001) (LAO) both deposited *via* molecular-beam epitaxy (MBE).[47,48] The PLD source material was a disk of single-crystal YAP:Ce (0.55 wt % Ce, CRYTUR), and the laser pulses were generated by a Lambda Physik KrF excimer source operating at a wavelength of 248 nm and pulse-rate of 2 Hz, with a fluence of approximately 0.7 J/cm^2. The substrates were held at 750 °C in a 1.0 mTorr O_2 atmosphere during the growth and subsequently cooled at a rate of 10 °C/min. For comparison, films of YAP:Ce were also grown on bulk crystalline LAO substrates under the same conditions.

As elaborated in the Supporting Information, films were characterized using Rutherford backscattering (RBS) (Supporting Information Figure S4); X-ray diffractometry (XRD) $\theta - 2\theta$ scans (Supporting Information Figure S1), rocking curves (Supporting Information Figure S3) and reciprocal space maps (Supporting Information Figure S2); atomic force microscopy (AFM) (Supporting Information Figure S5); optical profilometry; and steady state and time-resolved fluorimetry (Supporting Information Figures S6 and S7).

Cathodoluminescence (CL) emission spectra were measured with a modified Zeiss Gemini SUPRA 55 Scanning Electron Microscope (SEM), fitted with a spectrometer consisting of an Acton 2300i monochromator (150 line/mm, 500-nm blazed grating) and Andor Newton electron-multiplied CCD. A multimode optical fiber with a diameter of 200 μm inside of the SEM was used to couple the light directly from the sample surface to the spectrometer. To measure photon counts, a nickel parabolic reflector was positioned above the sample in order to couple a 1.3π solid angle of emission onto a photomultiplier tube outside of the vacuum chamber (Supporting Information Figure S13). To determine the total emission power from the films, back-reflections on the order of 50% off of the silicon substrate were also taken into account, as elaborated in the Supporting Information. A high contrast calibration sample of gold crystallites on highly ordered pyrolytic graphite (HOPG) was used to determine the diameter of the electron beam at each set of beam parameters used, based on the slope spanning 80−20% of the signal change. To determine the active volume of the electrons inside of the YAP:Ce layer, Monte Carlo simulations using the program CASINO 2.48 were performed (Supporting Information Figure S8 and S9).[50]

YAP:Ce films were patterned by quenching luminescence through exposure to a focused Ga^+ ion beam (FEI Quanta). The 200-nm silica beads (Corpuscular), deposited on the film out of aqueous solution, masked the gallium beam. After milling, the beads were removed with soaking in 1% Hellmanex, acetone, and deionized H_2O.

Conflict of Interest: The authors declare no competing financial interest.

Supporting Information Available: Characterization of the physical and optical properties of the YAP:Ce films; Monte Carlo simulations of electron scattering using CASINO; calculation of near-field energy transfer rates and intensities; calculation of emission rate per Ce ion; spectral properties of YAP:Ce grown on bulk crystal lanthanum aluminate; additional information regarding nanostructuring of YAP:Ce films; and an explanation of the CL collection apparatus. This material is available free of charge *via* the Internet at http://pubs.acs.org.

Acknowledgment. YAP:Ce film deposition was supported by the Chemical Sciences, Geosciences and Biosciences Division, Office of Basic Energy Sciences, Office of Science, U.S. Department

of Energy, FWP number SISGRKN. CL characterization and nanofabrication were supported by the National Science Foundation under Grant Number 1152656. CL, AFM and time-resolved fluorescence at the LBL Molecular Foundry were supported by the Office of Science, Office of Basic Energy Sciences, of the U.S. Department of Energy under Contract No. DE-AC02-05CH11231. C.A. and D.G.S. acknowledge support under the AFOSR Grant No. FA9550-10-1-0123, C.G.B. acknowledges an NSF Graduate Research Fellowship (DGE 1106400), and N.S.G. acknowledges a David and Lucile Packard Fellowship for Science and Engineering. We thank the P. Yang group for use of their XRD and the G. R. Fleming group for use of their fluorimeter. N.S.G. also thanks T. G. Ristroph for scintillating discussions.

REFERENCES AND NOTES

1. Hell, S. W. Far-Field Optical Nanoscopy. *Science* **2007**, *316*, 1153–1158.
2. Gustafsson, M. G. L. Nonlinear Structured-Illumination Microscopy: Wide-Field Fluorescence Imaging with Theoretically Unlimited Resolution. *Proc. Nat. Acad. Sci. U.S.A.* **2005**, *102*, 13081–13086.
3. Betzig, E.; Patterson, G. H.; Sougrat, R.; Lindwasser, O. W.; Olenych, S.; Bonifacino, J. S.; Davidson, M. W.; Lippincott-Schwartz, J.; Hess, H. F. Imaging Intracellular Fluorescent Proteins at Nanometer Resolution. *Science* **2006**, *313*, 1642–1645.
4. Rust, M. J.; Bates, M.; Zhuang, X. Sub-Diffraction-Limit Imaging by Stochastic Optical Reconstruction Microscopy (STORM). *Nat. Methods* **2006**, *3*, 793–796.
5. Hess, S. T.; Girirajan, T. P. K.; Mason, M. D. Ultra-High Resolution Imaging by Fluorescence Photoactivation Localization Microscopy. *Biophys. J.* **2006**, *91*, 4258–4272.
6. Lewis, A.; Isaacson, M.; Harootunian, A.; Muray, A. Development of a 500 Å Spatial Resolution Light Microscope: I. Light Is Efficiently Transmitted Through λ/16 Diameter Apertures. *Ultramicroscopy* **1984**, *13*, 227–231.
7. Pohl, D. W.; Denk, W.; Lanz, M. Optical Stethoscopy: Image Recording with Resolution λ/20. *Appl. Phys. Lett.* **1984**, *44*, 651–653.
8. Betzig, E.; Trautman, J. K.; Harris, T. D.; Weiner, J. S.; Kostelak, R. L. Breaking the Diffraction Barrier: Optical Microscopy on a Nanometric Scale. *Science* **1991**, *251*, 1468–1470.
9. Hartschuh, A.; Sánchez, E. J.; Xie, X. S.; Novotny, L. High-Resolution Near-Field Raman Microscopy of Single-Walled Carbon Nanotubes. *Phys. Rev. Lett.* **2003**, 095503-1–095503-9.
10. Mansfield, S. M.; Kino, G. S. Solid Immersion Microscope. *Appl. Phys. Lett.* **1990**, *57*, 2615–2616.
11. Levene, M. J.; Korlach, J.; Turner, S. W.; Foquet, M.; Craighead, H. G.; Webb, W. W. Zero-Mode Waveguides for Single-Molecule Analysis at High Concentrations. *Science* **2003**, *299*, 682–686.
12. Genet, C.; Ebbesen, T. W. Light in Tiny Holes. *Nature* **2007**, *445*, 39–46.
13. Schuck, P. J.; Fromm, D. P.; Sundaramurthy, A.; Kino, G. S.; Moerner, W. E. Improving the Mismatch Between Light and Nanoscale Objects with Gold Bowtie Nanoantennas. *Phys. Rev. Lett.* **2005**, *94*, 017402.
14. Mühlschlegel, P.; Eisler, H.-J.; Martin, O. J. F.; Hecht, B.; Pohl, D. W. Resonant Optical Antennas. *Science* **2005**, *308*, 1607–1609.
15. Willets, K. A.; Duyne, R. P. Van Localized Surface Plasmon Resonance Spectroscopy and Sensing. *Annu. Rev. Phys. Chem.* **2007**, *58*, 267–297.
16. Novotny, L.; van Hulst, N. Antennas for Light. *Nat. Photonics* **2011**, *5*, 83–90.
17. Ebenstein, Y.; Mokari, T.; Banin, U. Quantum-Dot-Functionalized Scanning Probes for Fluorescence-Energy-Transfer-Based Microscopy. *J. Phys. Chem. B* **2004**, *108*, 93–99.
18. Cuche, A.; Masenelli, B.; Ledoux, G.; Amans, D.; Dujardin, C.; Sonnefraud, Y.; Mélinon, P.; Huant, S. Fluorescent Oxide Nanoparticles Adapted to Active Tips for Near-Field Optics. *Nanotechnology* **2009**, *20*, 015603.
19. Fleischer, M.; Zhang, D.; Braun, K.; Jäger, S.; Ehlich, R.; Häffner, M.; Stanciu, C.; Hörber, J. K. H.; Meixner, A. J.; Kern, D. P. Tailoring Gold Nanostructures for Near-Field Optical Applications. *Nanotechnology* **2010**, *21*, 065301.
20. Neumann, L.; Pang, Y.; Houyou, A.; Juan, M. L.; Gordon, R.; van Hulst, N. F. Extraordinary Optical Transmission Brightens Near-Field Fiber Probe. *Nano Lett.* **2011**, *11*, 355–360.
21. Bao, W.; Melli, M.; Caselli, N.; Riboli, F.; Wiersma, D. S.; Staffaroni, M.; Choo, H.; Ogletree, D. F.; Aloni, S.; Bokor, J.; *et al.* Mapping Local Charge Recombination Heterogeneity by Multidimensional Nanospectroscopic Imaging. *Science* **2012**, *338*, 1317–1321.
22. Johnson, T. W.; Lapin, Z. J.; Beams, R.; Lindquist, N. C.; Rodrigo, S. G.; Novotny, L.; Oh, S.-H. Highly Reproducible Near-Field Optical Imaging with Sub-20-nm Resolution Based on Template-Stripped Gold Pyramids. *ACS Nano* **2012**, *6*, 9168–9174.
23. Autrata, R.; Schauer, P.; Kvapil, J.; Kvapil, J. A Single Crystal of $YAlO_3$: Ce^{3+} as a Fast Scintillator in SEM. *Scanning* **1983**, *5*, 91–96.
24. Yacobi, B. G.; Holt, D. B. *Cathodoluminescence Microscopy of Inorganic Solids*; Plenum Press: New York, 1990.
25. Yamamoto, N.; Araya, K.; García de Abajo, F. J. Photon Emission from Silver Particles Induced by a High-Energy Electron Beam. *Phys. Rev. B* **2001**, *64*, 205419.
26. Vesseur, E. J. R.; de Waele, R.; Kuttge, M.; Polman, A. Direct Observation of Plasmonic Modes in Au Nanowires Using High-Resolution Cathodoluminescence Spectroscopy. *Nano Lett.* **2007**, *7*, 2843–2846.
27. Chaturvedi, P.; Hsu, K. H.; Kumar, A.; Fung, K. H.; Mabon, J. C.; Fang, N. X. Imaging of Plasmonic Modes of Silver Nanoparticles Using High-Resolution Cathodoluminescence Spectroscopy. *ACS Nano* **2009**, *3*, 2965–2974.
28. Coenen, T.; van de Groep, J.; Polman, A. Resonant Modes of Single Silicon Nanocavities Excited by Electron Irradiation. *ACS Nano* **2013**, *7*, 1689–1698.
29. Degiron, A.; Lezec, H. J.; Yamamoto, N.; Ebbesen, T. W. Optical Transmission Properties of a Single Subwavelength Aperture in a Real Metal. *Opt. Commun.* **2004**, *239*, 61–66.
30. Lim, S. K.; Brewster, M.; Qian, F.; Li, Y.; Lieber, C. M.; Gradečak, S. Direct Correlation Between Structural and Optical Properties of III–V Nitride Nanowire Heterostructures with Nanoscale Resolution. *Nano Lett.* **2009**, *9*, 3940–3944.
31. Li, Q.; Wang, G. T. Spatial Distribution of Defect Luminescence in GaN Nanowires. *Nano Lett.* **2010**, *10*, 1554–1558.
32. Inami, W.; Nakajima, K.; Miyakawa, A.; Kawata, Y. Electron Beam Excitation Assisted Optical Microscope with Ultra-High Resolution. *Opt. Express* **2010**, *18*, 12897–12902.
33. Chiba, A.; Tanaka, S.; Inami, W.; Sugita, A.; Takada, K.; Kawata, Y. Amorphous Silicon Nitride Thin Films Implanted with Cerium Ions for Cathodoluminescent Light Source. *Opt. Mater.* **2013**, *35*, 1887–1889.
34. Yoon, H. P.; Lee, Y.; Bohn, C. D.; Ko, S.-H.; Gianfrancesco, A. G.; Steckel, J. S.; Coe-Sullivan, S.; Talin, A. A.; Zhitenev, N. B. High-Resolution Photocurrent Microscopy Using Near-Field Cathodoluminescence of Quantum Dots. *AIP Adv.* **2013**, *3*, 062112.
35. Wojtowicz, A. J. Rare-Earth-Activated Wide Bandgap Materials for Scintillators. *Nucl. Instrum. Methods Phys. Res., Sect. A* **2002**, *486*, 201–207.
36. Baccaro, S.; Blažek, K.; de Notaristefani, F.; Maly, P.; Mares, J.; Pani, R.; Pellegrini, R.; Soluri, A. Scintillation Properties of YAP:Ce. *Nucl. Instrum. Methods Phys. Res., Sect. A* **1995**, *361*, 209–215.
37. Weber, M. J. Optical Spectra of Ce^{3+} and Ce^{3+}-Sensitized Fluorescence in $YAlO_3$. *J. Appl. Phys.* **1973**, *44*, 3205–3208.
38. Ponce, F. A.; Bour, D. P.; Götz, W.; Wright, P. J. Spatial Distribution of the Luminescence in GaN Thin Films. *Appl. Phys. Lett.* **1996**, *68*, 57–59.
39. Ravichandran, D.; Roy, R.; Chakhovskoi, A. G.; Hunt, C. E.; White, W. B.; Erdei, S. Fabrication of $Y_3Al_5O_{12}$:Eu Thin Films and Powders for Field Emission Display Applications. *J. Lumin.* **1997**, *71*, 291–297.
40. Šonský, J.; Lančok, J.; Jelínek, M.; Oswald, J.; Studnička, V. Growth of Active Nd-Doped YAP Thin-Film Waveguides by

Laser Ablation. *Appl. Phys. A: Mater. Sci. Process.* **1998**, *66*, 583–586.
41. Cho, K. G.; Kumar, D.; Holloway, P. H.; Singh, R. K. Luminescence Behavior of Pulsed Laser Deposited Eu:Y_2O_3 Thin Film Phosphors on Sapphire Substrates. *Appl. Phys. Lett.* **1998**, *73*, 3058–3060.
42. Nakanishi, Y.; Miyake, A.; Kominami, H.; Aoki, T.; Hatanaka, Y.; Shimaoka, G. Preparation of ZnO Thin Films for High-Resolution Field Emission Display by Electron Beam Evaporation. *Appl. Surf. Sci.* **1999**, *142*, 233–236.
43. Gurumurugan, K.; Chen, H.; Harp, G. R.; Jadwisienczak, W. M.; Lozykowski, H. J. Visible Cathodoluminescence of Er-Doped Amorphous AlN Thin Films. *Appl. Phys. Lett.* **1999**, *74*, 3008–3010.
44. Toro, R. G.; Malandrino, G.; Fragalà, I. L.; Keshu, W.; Leto, A.; Pezzotti, G. Cathodoluminescence Investigation of Residual Stress in Er^{3+}:$YAlO_3$ Thin Films Grown on (110) $SrTiO_3$ Substrate by Metal-Organic Chemical Vapor Deposition. *J. Phys. Chem. B* **2006**, *110*, 23977–23981.
45. Ŗemsa, J.; Jelinek, M.; Kocourek, T.; Oswald, J.; Studnička, V.; Čerňanský, M.; Uherek, F.; Jelínek, M. Highly Oriented Crystalline Er:YAG and Er:YAP Layers Prepared by PLD and Annealing. *Appl. Surf. Sci.* **2009**, *255*, 5292–5294.
46. Kumaran, R.; Webster, S. E.; Penson, S.; Li, W.; Tiedje, T. Molecular Beam Epitaxy Growth of Neodymium-Doped Yttrium Aluminum Perovskite. *J. Cryst. Growth* **2009**, *311*, 2191–2194.
47. Warusawithana, M. P.; Cen, C.; Sleasman, C. R.; Woicik, J. C.; Li, Y.; Kourkoutis, L. F.; Klug, J. A.; Li, H.; Ryan, P.; Wang, L.-P.; *et al.* A Ferroelectric Oxide Made Directly on Silicon. *Science* **2009**, *324*, 367–370.
48. Warusawithana, M. P.; Richter, C.; Mundy, J. A.; Roy, P.; Ludwig, J.; Paetel, S.; Heeg, T.; Pawlicki, A. A.; Kourkoutis, L. F.; Zheng, M.; *et al.* $LaAlO_3$ Stoichiometry is Key to Electron Liquid Formation at $LaAlO_3$/$SrTiO_3$ Interfaces. *Nat. Commun.* **2013**, *4*, 3351.1–9.
49. Wisniewska, M.; Wojtowicz, A. J.; Lukasiewicz, T.; Frukacz, Z.; Galazka, Z.; Malinowski, M. Radio- and VUV-Excited Luminescence of YAP:Ce, YAP:Pr and YAG:Pr. *Proc. SPIE* **2001**, *4412*, 351–356.
50. Drouin, D.; Couture, A. R.; Joly, D.; Tastet, X.; Aimez, V.; Gauvin, R. CASINO V2.42—A Fast and Easy-to-Use Modeling Tool for Scanning Electron Microscopy and Microanalysis Users. *Scanning* **2007**, *29*, 92–101.
51. Villarrubia, J. S.; Ding, Z. J. Sensitivity of SEM Width Measurements to Model Assumptions. *Proc. SPIE* **2009**, *7272*, 72720R.
52. Eshelby, J. D.; Newey, C. W. A.; Pratt, P. L.; Lidiard, A. B. Charged Dislocations and the Strength of Ionic Crystals. *Philos. Mag.* **1958**, *3*, 75–89.
53. Rhodes, W. H.; Kingery, W. D. Dislocation Dependence of Cationic Diffusion in $SrTiO_3$. *J. Am. Ceram. Soc.* **1966**, *49*, 521–526.
54. Baryshevsky, V. G.; Korzhik, M. V.; Minkov, B. I.; Smirnova, S. A.; Fyodorov, A. A.; Dorenbos, P.; van Eijk, C. W. E. Spectroscopy and Scintillation Properties of Cerium Doped $YAlO_3$ Single Crystals. *J. Phys.: Condens. Matter* **1993**, *5*, 7893.
55. Özen, G.; Demirata, B. Energy Transfer Characteristics of the Hydrogen Peroxide Induced Ce^{3+}-Ce^{4+} Mixture. *Spectrochim. Acta, Part A* **2000**, *56A*, 1795–1800.